Iranian Journal of Chemistry and Chemical Engineering (IJCCE)

Environmentally Friendly Synthesis of Hydrophobic $CaCO_3$ Nanoparticles from Paper Waste: A Facile Approach

Hamid Kazemi Hakki[*1,2], Aref Ghaderi[3], Pouya Nagshini[3,4]

1. *Department of Chemical Engineering, Faculty of Engineering, Soran University, Soran, Erbil, Kurdistan Region, Iraq. (hamid_kazemi_eng@hotmail.com, hamid.kazemihaki@visitors.soran.edu.iq)*
2. *Nuzhan Nanofannavar Company, West Azerbaijan Science and Technology Park, Urmia, Iran.*
3. *Department of Civil Engineering, Faculty of Engineering, Soran University, Soran, Erbil, Kurdistan Region, Iraq.*
4. *Department of Cellular and Molecular, Biological Sciences and Technologies, Islamic Azad University Branch of Urmia, Urmia, Iran.*

Abstract

At present, the escalating magnitude of waste represents a formidable global concern, wherein paper waste alone constitutes approximately 26% of the overall waste deposited in landfills. Thus, the transformation of paper waste into viable products assumes paramount significance. In this study, paper waste was converted to $CaCO_3$ using a thermal process and surface-modified with stearic acid. The effect of environmental pH and process temperature on the crystalline structure and morphology of the product was evaluated. The prepared $CaCO_3$ was used in deactivation of gram-negative agrobacterium tumefaciens and the effect of hydrophobicity on the $CaCO_3$ antibacterial activity was studied. XRD, SEM, FTIR, BET/BJH, contact angle and TEM characterization techniques were utilized to characterize structure and physicochemical properties of prepared $CaCO_3$. According to the XRD analysis, the optimal temperature for the conversion process was 500°C in an air environment without any changes in pH. SEM analysis confirmed that as the calcination temperature increased, the number of cracks and holes on the surface also increased. BET analysis confirmed this by showing a decrease in the specific surface area in the Ca-750 sample. TEM analysis revealed nanoparticles with spherical and irregular spherical geometries, ranging in size from 30 to 90 nm. According to the contact angle analysis, increasing the concentration of stearic acid led to an increase in the contact angle to 121.4°. This increase in contact angle indicates an enhancement in the hydrophobicity of the prepared nanoparticles, which had a synergistic effect on their antibacterial activity. The antibacterial activity test of both prepared hydrophilic and hydrophobic $CaCO_3$ depicted the high antibacterial activity of both $CaCO_3$ while the hydrophobic $CaCO_3$ revealed higher antibacterial activity compared to hydrophilic $CaCO_3$.

Keywords: Paper Waste, Conversion Process, $CaCO_3$, Surface Modification, Hydrophobic Nanoparticles, Antibacterial Activity.

1 INTRODUCTION

The generation of diverse waste types, encompassing plastic, paper, and alloys, poses a formidable challenge in the contemporary world. Recent data reveals that paper accounts for approximately 26% of the total waste found in landfills [1]. Meanwhile, despite the advent of electronic devices such as mobile phones, tablets, and laptops, along with the growing popularity of electronic books, the utilization of paper has not diminished [2, 3]. Paper waste comprises various forms, including books, packaging cardboard, newspapers, and Kraft paper [4]. Composed of cellulose, hemicellulose, lignin, and calcium carbonate, paper possesses the potential to be transformed into valuable products through appropriate methodologies that leverage its constituent components [5].

Every year, a vast quantity of paper is manufactured worldwide to satisfy the demands of both society and industries. Regrettably, the consequential paper waste poses a significant environmental hazard, as its decomposition releases methane gas, which is 25 times more potent as a greenhouse gas than carbon dioxide (CO2) [6]. Converting paper waste and utilizing the resulting products serve a dual purpose. Firstly, it helps to reduce environmental pollution by effectively managing paper waste. Secondly, the products derived from paper waste conversion can be employed in wastewater treatment processes, thereby enhancing their practical applicability. This dual approach not only addresses the issue of environmental pollution but also contributes to the improvement of wastewater treatment methods [7, 8].

Several studies have reported on the conversion of paper wastes into valuable products such as cellulose fibres, nanocellulose, biofuels, bio-hydrogen, lightweight concrete aggregates, and soil amendments [9, 10].

Yu et al.[11] extracted cellulose nanocrystals from paper waste of egg trays using a chemical and mechano-ball milling process. According to the results, the highest extraction of nanocellulose with 88.2% crystallinity was achieved using an alkali-acid (NaOH(10%)-H_2SO_4(65%)) method. Egamberdiev et al.[12] extracted cellulose nanocrystals from paper waste using hydrolysis method in order to enhance the physical properties of paper sheets. Their obtained nanocellulose had 10 to 30 nm diameter and improved the tear resistance strength, traction and burst indices of paper sheets.

Durairaj et al.[13] synthesized activated carbon from two different tissue paper and hardboard sources and used it as an adsorbent in the removal of methylene blue. Their results revealed that the activated carbon derived from tissue paper had a higher adsorption capacity than the activated carbon derived from hardboard.

Ye et al.[14] studied the conversion of paper waste to graphene-tethered carbon fiber composite. For this purpose, they used urea as a carbonization additive, and the use of urea led to excellent increases in electrical conductivity. They prepared a graphene-tethered carbon fiber/polydimethyl siloxane composite to use as a membrane for oil-water separation. The prepared hydrophobic membrane exhibited high oil-water separation capacity.

Converting paper waste into valuable Calcium-based materials, such as $CaCO_3$, Alginate-$CaSiO_3$ polymers, carboxymethylcellulose calcium, and calcium alginate-carboxymethyl cellulose, can be a useful method for addressing challenges in various fields [15, 16].

$CaCO_3$ nanoparticles are cost-effective materials with low toxicity, high biocompatibility, and cytocompatibility. This material is utilized in various fields such as wastewater treatment, environmental applications, drug delivery and controlled release, hydrophobic coatings, and antibacterial coatings. These nanoparticles offer significant advantages due to their unique properties [17-19].

Al-Azzawi et al. synthesized $CaCO_3$ nanoparticles from chicken eggshells and utilized the prepared nanoparticles for the deactivation of Acinetobacter baumannii, Klebsiella pneumoniae, Staphylococcus aureus, Burkholderia cepacia, Pseudomonas aeruginosa, Proteus mirabilis, and E. coli. Their results indicated that the prepared $CaCO_3$ nanoparticles exhibited excellent efficacy in deactivating the mentioned bacteria. Moreover, the prepared nanoparticles hold potential applications in dental fillings and bone repair [20].

This research focuses on the conversion of paper waste into $CaCO_3$ nanoparticles using an inexpensive, facile, and rapid method. The aim is to address waste management and reduce environmental pollution challenges, while also recognizing the potential value of paper waste for $CaCO_3$ nanoparticle production, rather than considering it as mere garbage. The study investigated the effects of pH and temperature on the conversion process and the characteristics of the final product. Furthermore, the surface-modified $CaCO_3$ nanoparticles were utilized for deactivating gram-negative Agrobacterium tumefaciens.

2. Material and Methods

2.1 Material

The reagents used in this study Potassium hydroxide and HCl were purchased from Sigma Aldrich Company. Distilled water was purchased from Dr. Mojallali Company. All the reagents were used as received without any further purification

2.2 $CaCO_3$ nanoparticles Preparation

The $CaCO_3$ nanoparticles were synthesized from printed paper wastes. To achieve this, 15g the printed papers were crushed into small dimensions. The crushed paper waste was then transferred to a sealed porcelain dish and calcined at 500°C and 750°C at air for 2 h. In order to evaluate the effect of pH on the conversion of paper waste, the calcination process was performed at the 500°C and acidic and alkaline environment. To achieve this, the percentage of HCl and KOH was adjusted to 10 wt%. The samples were then subjected to calcination at temperatures of 500°C and 700°C, resulting in two sets of samples named Ca-500 and Ca-750, respectively. Additionally, samples prepared under acidic and alkaline conditions were named Ca-500-H and Ca-500-OH, respectively.

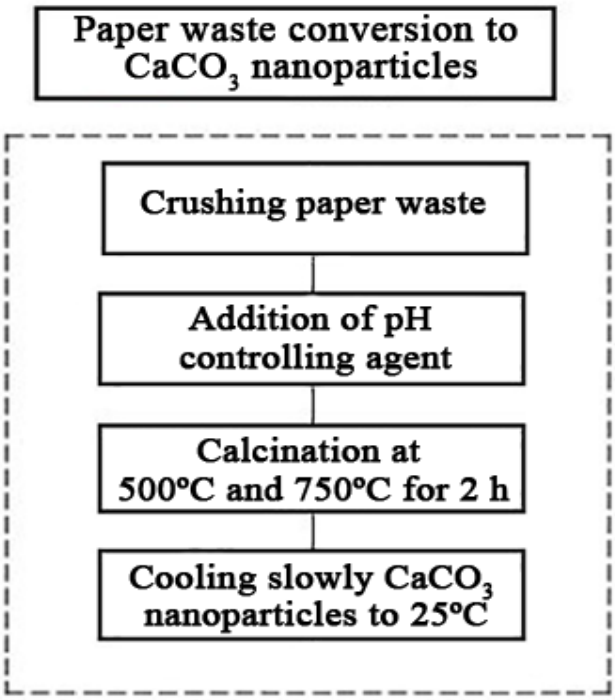

Figure 1. Schematic of paper waste conversion to $CaCO_3$ nanoparticles

2.3 Surface Modification of prepared $CaCO_3$

The surface modification of prepared $CaCO_3$ was performed using alcoholic stearic acid solution. For this purpose, three different concentrations of stearic acid in isopropyl alcohol (0.02, 0.04, 0.06 mol/L) were prepared. The aim of applying different concentration of stearic acid was evaluate the influence of different concentration of stearic acid on the surface hydrophobicity of $CaCO_3$ and optimization of stearic acid concentration and surface modification process. Then, 3 g of the produced $CaCO_3$ nanoparticles was immersed in 100 ml of each the respective solutions. The immersion process was carried out for 20 min with continuous stirring. After the immersion, the $CaCO_3$ nanoparticles were separated and was subjected to a drying process. The dying process was conducted in an oven at the 80°C for 3 h.

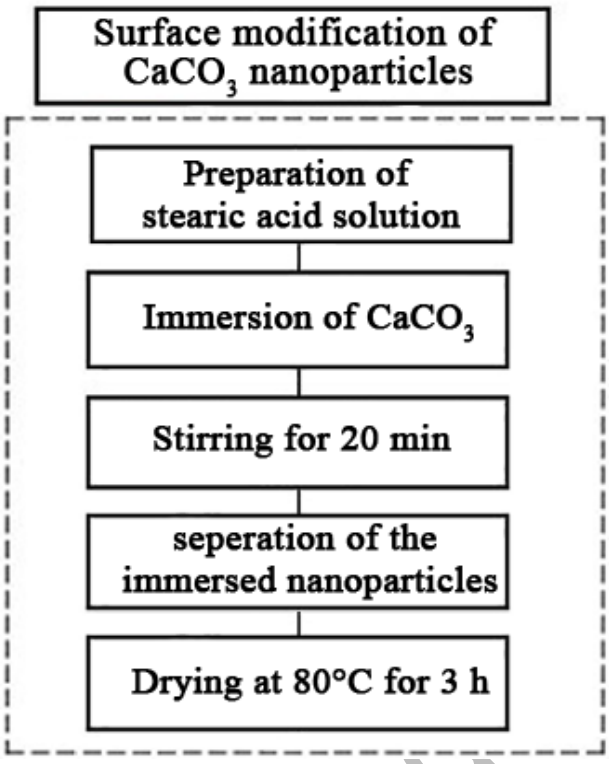

Figure 2. Schematic of surface modification of the prepared $CaCO_3$ nanoparticles

2.4 Nanocatalyst Characterization Techniques

In this research, the surface morphology and nanoparticle geometry of the prepared $CaCO_3$ samples were studied using a scanning electron microscope (SEM, Quanta 450). The crystalline structure and phase purity of the samples were characterized using X-ray diffraction (XRD) analysis, which was performed using a PANalytical X' Pert instrument equipped with Cu Kα = 1.5406 Å radiation (X'Pert³ MRD model). For this purpose, a Siemens D5000 diffractometer equipped with a Cu radiation source (wavelength of 0.154056 nm) was used, with a scanning speed of 0.02 s^{-1} and a 2θ range from 10 to 70. The specific surface area of the CaCO3 sample was evaluated using the BELSORP-mini analyzer, which employed the Brunauer-Emmett-Teller (BET) and Barrett-Joyner-Halenda (BJH) methods. The BET method involved a 35-point analysis equation to measure the physisorption of gas and derive the surface area of the sample. The BJH method was used to determine the pore size distribution of the sample. Fourier Transform Infrared Spectroscopy (FTIR) analysis was utilized by a PerkinElmer Spectrum 65 instrument at a wavelength range of 4000 to 400 cm^{-1} in order to identify the existence of functional groups in the sample. The contact angle and surface wettability of the samples were determined using the contact angle measuring device CA-ES20.

2.5 Evaluation of antibacterial activity of $CaCO_3$ nanoparticles

The disk diffusion method is a simple, inexpensive, and widely utilized method for evaluating the antibacterial activity of materials. This method involves placing a paper disk containing the test substance onto a bacterial lawn that has been seeded on the surface of an agar medium. Following this, the medium is incubated, and the zone of inhibition around the disk is measured to assess the susceptibility of the bacterial isolate to the test substance.

For the evaluation of the antibacterial activity of the prepared $CaCO_3$ nanoparticles against Gram-negative Agrobacterium tumefaciens, the disk diffusion method was employed on Mueller Hinton Agar medium. The bacterial solution was cultured on a nutrient agar medium according to the McFarland standard (1.5×10^8 cfu/ml). To prepare the Mueller Hinton Agar medium, 39 g of Mueller Hinton Agar powder was dissolved in deionized water and the medium was dispersed in plates after sterilization. The bacteria were cultured on Mueller Hinton medium and incubated in an incubator at 37ºC for 24 h to grow. Then, a uniform stable colloidal suspension of $CaCO_3$ nanoparticles with a concentration of 1000 mg/ml was prepared by suspending the prepared $CaCO_3$ nanoparticles in sterile normal saline under 30 w ultrasound irradiation in pulse mode for 20 min. Then, 0.05 and 0.1 ml of prepared nanoparticles suspension was added in discs and wells, respectively. A nanoparticle-free medium was used as control. The growth rate of the bacteria and the zone of inhibition was measured after 24 h incubation.

3. Results and Discussions

3.1 XRD Analysis

The XRD patterns of the products obtained from the paper waste calcination process at different temperatures and environments were recorded in the 2θ range of 20-80° and are presented in fig.1. The peaks observed at 23.04, 29.39, 35.99, 39.4, 43.15, 47.52, 48.50, 57.40, 60.71, and 64.73 are attributed to the $CaCO_3$ crystalline structure [14]. As shown in Fig.4, increasing the temperature to 750°C resulted in decreased peak intensity, and some peaks became wider compared to the same peaks in the sample calcined at 500°C. These results indicate that 500°C is the optimal temperature for producing $CaCO_3$ with high crystallinity from paper wastes. Furthermore, the acidic environment was found to affect the crystallinity by influencing the peak intensity. In contrast, the use of KOH as a pH modifier in the alkaline environment led to the decomposition of the $CaCO_3$ crystalline structure and the generation of the K_2CO_3 structure. The peak with high intensity at 72.4 is attributed to the K_2CO_3 structure that formed along with the $CaCO_3$ during the annealing process in the alkaline environment [21]. Overall, the results revealed that neither an acidic nor an alkaline environment is suitable for the formation of $CaCO_3$ from the paper waste annealing process.

The average crystallite size of the prepared samples was calculated using Debye–Scherer equation [22] :

$$d = \frac{K\lambda}{\beta COS\theta}$$

Where d represents the crystalline size, K denotes the Scherrer constant (typically ranging between 0.9 and 1.0), β represents the full width at half maximum (FWHM) of the peak, λ represents the wavelength of the applied X-ray, and θ represents the Bragg angle. According to the Debye–Scherer equation, the crystallite size of Ca-500, Ca-750, Ca-500-H, and Ca-500-OH were 42.32, 32.66, 35.73, and 19.28 nm, respectively. The lattice strains of Ca-500, Ca-750, Ca-500-H, and Ca-500-OH were calculated to be 0.0022752, 0.0031357, 0.0044314, and 0.0076811, respectively. These results indicate that the lattice strain increases with higher calcination temperature, particularly at 750°C. Moreover, the lattice strain shows a significant increase in both acidic and alkaline pH conditions, with the alkaline sample exhibiting the highest increase.

Fig.1 provides a clear visualization of the observed trend, showing a decrease in XRD peak intensities with increasing temperature and in alkaline pH conditions. Notably, in the alkaline pH, this decrease in intensity is

accompanied by broader peaks. These findings suggest that the increasing lattice strain contributes to the broadening and weakening of diffraction peaks in X-ray diffraction patterns. This phenomenon points to a distortion or deformation in the crystal lattice structure, affecting the arrangement of atoms or crystalline planes within the material [17].

To furthermore evaluation of calcination temperature and environment pH effects on the crystalline structure and lattice of prepared $CaCO_3$ nanoparticles, the Bragg's equation was utilized. According to the Bragg's equation the interlayer spacing of Ca-500, Ca-750, Ca-500-H, and Ca-500-OH samples were 0.17459, 0.190628, 0.20163, and 0.24647 nm, respectively. The results revealed that the interlayer spacing in the $CaCO_3$ lattice was increased by increased temperature to 750°C and converting environment pH. While in the alkaline environment the interlayer spacing considerably increased. This means distance between layers in the $CaCO_3$ lattice increased and this is due the distortion in the $CaCO_3$ crystalline structure [23, 24].

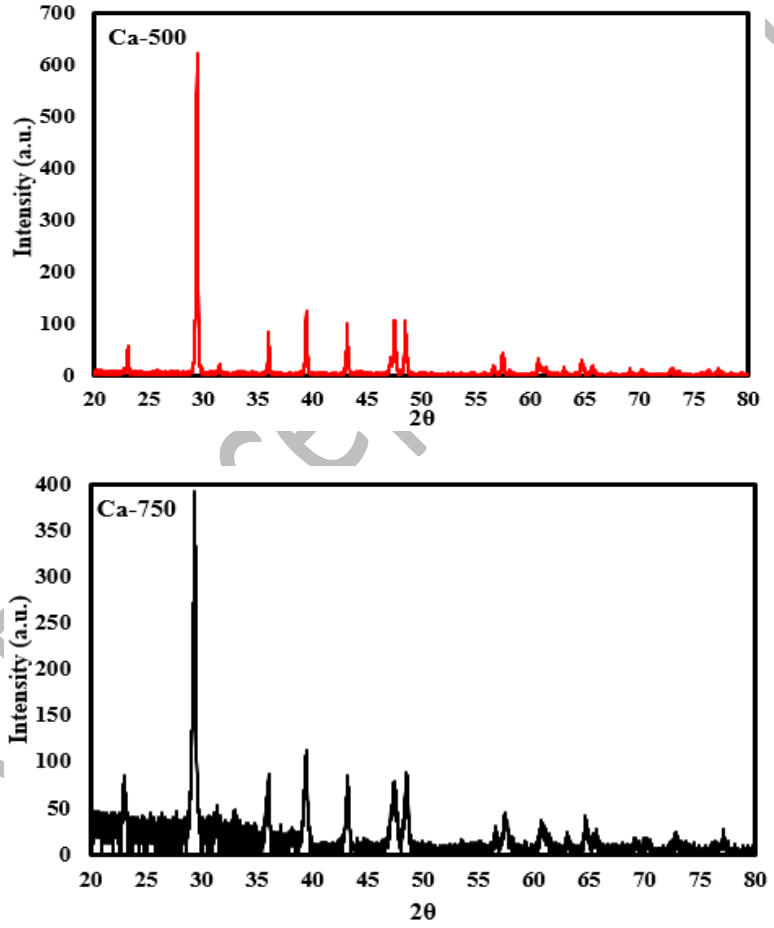

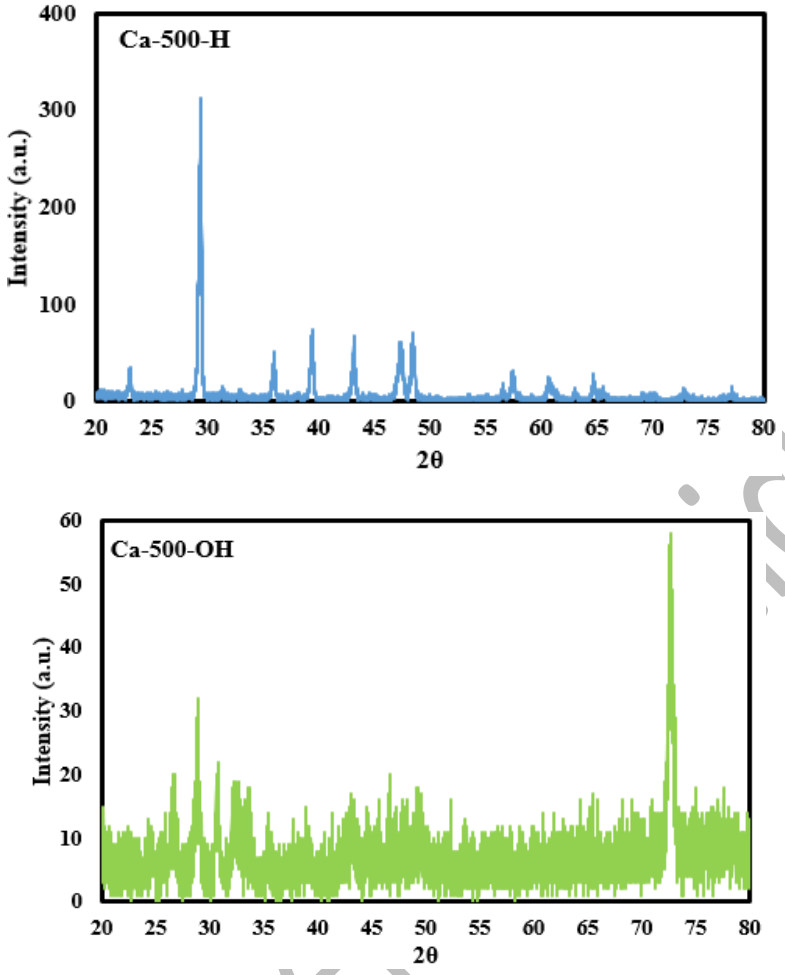

Figure 3. XRD patterns of the samples calcined at 500C (Ca-500), 750C (Ca-750), acidic pH (H-500-OH), and alkaline pH (H-500-OH)

3.2 SEM Analysis of Photocatalytic Composites

Due to the aim of this research is converting paper wastes to $CaCO_3$ nanoparticles, the SEM analysis was applied to study the morphology and nanoparticles geometry of prepared $CaCO_3$ and effect the calcination temperature on the morphology of prepared $CaCO_3$. Fig.2 shows that both the Ca-500 and Ca-750 samples the nanoparticles had been formed in spherical shapes. SEM analysis confirmed the good morphology and homogeneous surface of the Ca-500 sample, with relatively homogeneous particle distribution. By utilizing Image J software and analyzing SEM images, the results revealed that the nanoparticles exhibited sizes ranging from 50 to 85 nm. However, increasing the calcination temperature from 500°C to 750°C resulted in the generation of cracks and holes on the surface of the prepared $CaCO_3$, which were distributed all over the surface of the Ca-750 sample. This can causes a decrease in the surface area of the Ca-750 sample. The SEM analysis indicated the moderately rough surface of the Ca-500 sample, confirming the porous nature of the prepared sample, which is advantageous for the antibacterial effectiveness of the sample. To compare the results with another studies that synthesized $CaCO_3$ using various method and sources was shown in Table.1.

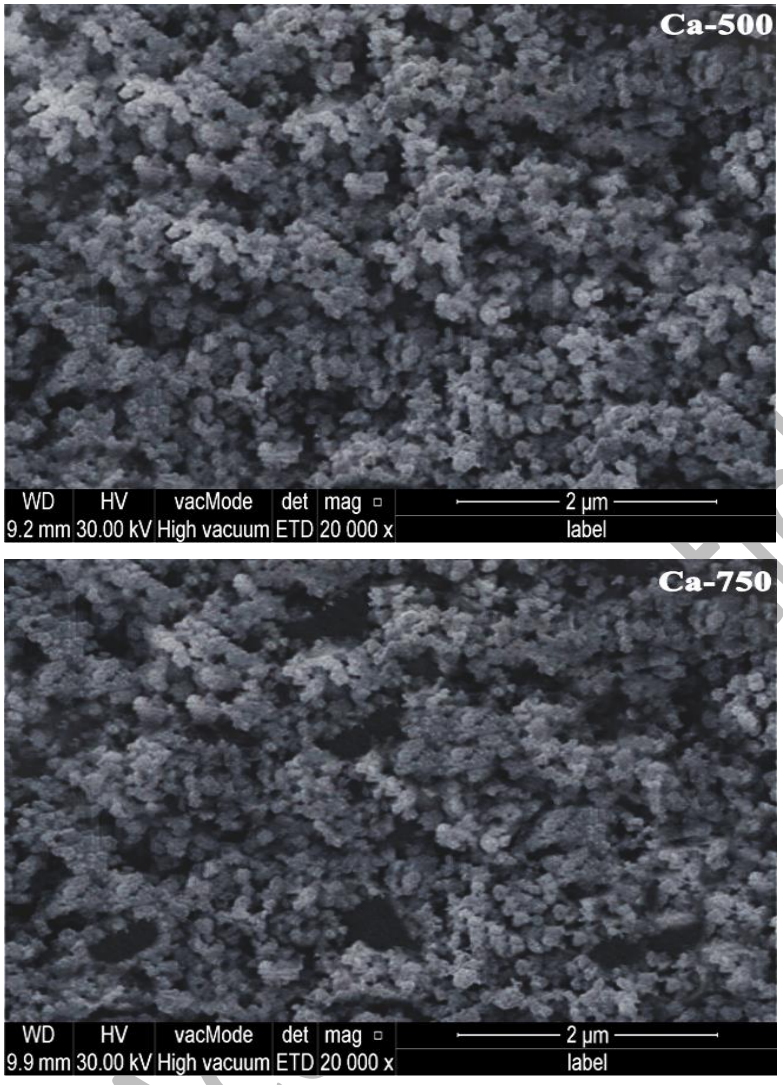

Figure 4. SEM images of prepared $CaCO_3$ nanoparticles at 500°C (Ca-500) and 750°C (Ca-750) in the neutral pH

	Synthesis method	Source	particles size	Surface Area (m^2/g)	Reference
1	Crushing the shell & sieving	Chicken egg shell	31 – 34 nm	-	[20]
2	Ball Milling Mechanochemistry Process	Seashells (clam shell)	1 – 35 µm	7.3	[25]
3	sol–gel method	Cockle Shells	39 nm	26	[26]
4	Carbonation of the CaO	CaO	40 – 200 nm	-	[27]
5	Precipitation & carbonation methods	Quicklime	0.5 - 2.7 µm	-	[28]
6	Precipitation method	Egg shell	4 – 6 µm	-	[29]

3.3 BET Analysis of $CaCO_3$ nanoparticles

BET analysis was utilized in order to evaluate the effect of the calcination temperature on the surface area of prepared $CaCO_3$ from paper wastes. The specific surface area of the synthesized $CaCO_3$ nanoparticles was determined using the Brunauer-Emmett-Teller (BET) theory. The BET equation is given by:

$$\frac{1}{X[\left(\frac{P_0}{P}\right)-1]}=\frac{1}{X_mC}+\frac{C-1}{X_mC}\left(\frac{P}{P_0}\right)$$

Where X represents the fractional coverage of the solid surface by adsorbed gas molecules, Xm is the monolayer coverage, C is a constant related to the heat of adsorption, and P0 is the saturation vapor pressure of the adsorbate at the experimental temperature. Gas adsorption measurements were performed at various equilibrium pressures, and the BET equation was applied to the experimental data to estimate the specific surface area of the $CaCO_3$ nanoparticles.

According to the BET analysis the surface area of the Ca-500 and Ca-750 samples, as determined by BET analysis, was 27.318 and 12.627 m^2/g, respectively. The BET analysis showed that the surface area of the Ca-750 sample decreased as the calcination temperature increased to 750°C. This decrease in surface area was due to the presence of cracks and holes on the surface of the Ca-750 samples. The SEM and XRD analyses were in good agreement with the BET analysis. Fig.3 shows the adsorption and desorption plots of Ca-500 and Ca-750. The hysteresis type of the adsorption and desorption plots is H1, indicating a cylindrical pore geometry of the prepared $CaCO_3$ from paper waste conversion. The results of this investigation align with previous research that has documented a decline in the specific surface area of nanomaterials as the calcination temperature rises. This phenomenon is also accompanied by alterations in pore size and structure.

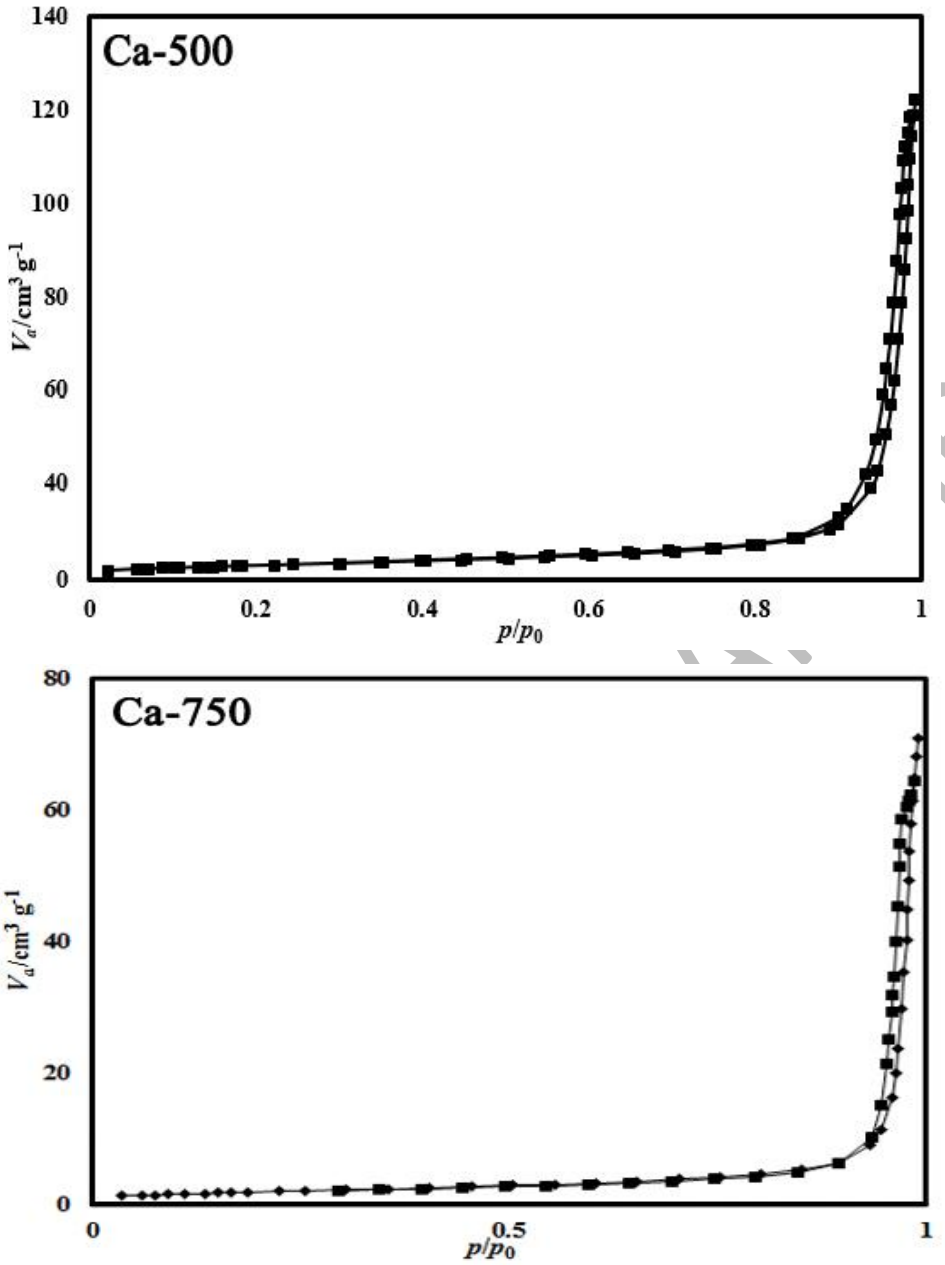

Figure 5. Adsorption-desorption-Plot of prepared nanoparticles at 500°C (Ca-500) and 750°C (Ca-750) in the neutral pH

3.4 FTIR analysis

To further characterize the prepared $CaCO_3$ samples, FTIR analysis was performed to identify the functional groups present in the samples and to evaluate the effect of the calcination temperature on these groups. $CaCO_3$ exhibits four characteristic absorption bands, which are divided into two ranges: 1000-500 cm^{-1} and 1500-1000 cm^{-1} [30]. The FTIR patterns reveal peaks at 1470, 1120, 834, and 725 cm^{-1}, corresponding to the in-plane bending, out-of-plane bending, symmetric stretch, and asymmetric stretch of the carbonate ion, respectively [31, 32]. The peak observed at 2310 cm^{-1} is attributed to the CO_2 absorption band, which may be due to the occurrence of a

combustion reaction during the calcination process and absorbed by the samples [33]. The appeared absorption bands at 2956 and 2806 cm^{-1} can be attributed to C-H asymmetric and symmetric stretching vibrations [34, 35].

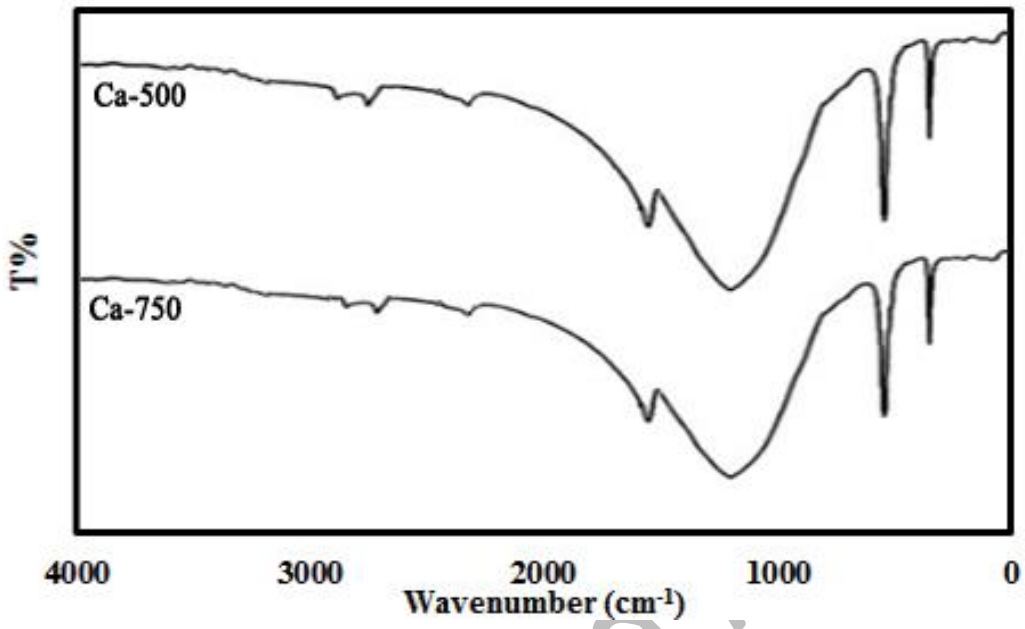

Figure 6. FTIR analysis of prepared nanoparticles at 500°C (Ca-500) and 750°C (Ca-750) in the neutral pH

3.5 Contact angle analysis

The Ca-500 sample was chosen as the optimal sample and the surface modification process was conducted on this sample by using alcoholic stearic acid solution with different concentrations. The results, shown in Fig.5, indicate that the contact angles obtained at concentrations of 0.02, 0.04, and 0.06 mol/L were 100.3°, 112.5°, and 121.4°, respectively. According to the results by increasing the stearic acid solution from 0.02 to 0.06 mol/L the contact angle increased from 100.3° to 121.4°. As shown in fig.5 the contact angle analysis confirms the effective role of stearic acid in increasing the contact angle and decreasing wettability of Ca-500 sample. The sample was prepared by 0.06 mol/L of alcoholic solution was chosen to conduct the antibacterial activity. Indeed, stearic acid modified the surface of $CaCO_3$ by decreasing its polarity and makes it hydrophobic. The surface modification of $CaCO_3$ includes the attaching of stearic acid onto the surface of the synthesized $CaCO_3$ nanoparticles. During the surface modification of the prepared $CaCO_3$ nanoparticles, the polarity of CaCO3 is reduced by chemically binding the hydrophilic head of stearic acid to its polar surface. This process enhances the hydrophobicity and water repellency of the $CaCO_3$ surface by decreasing its polarity. The synergistic effect of hydrophobic nanoparticles' hydrophobicity on their antibacterial activity is due to their accumulation at the air-water interface, where the bacterial cell membrane is located [36].

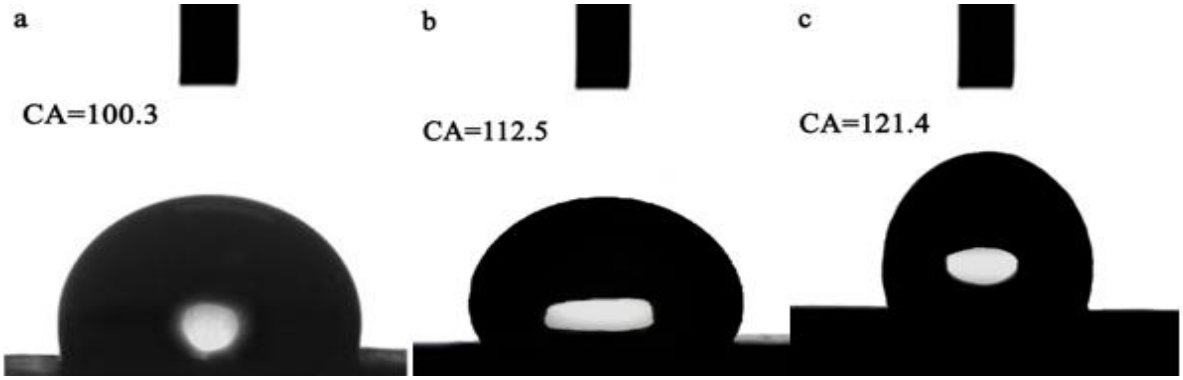

Figure 7. Contact angle analysis of surface modified $CaCO_3$ with (a) 0.02 mol/L (b) 0.04 mol/L (c) 0.06 mol/L of stearic acid

3.6 TEM Analysis

TEM analysis was utilized to further specify the prepared $CaCO_3$ nanoparticles. Fig.6 indicates the TEM image of the Ca-500 sample. TEM analysis illustrates the presence of particles in both spherical and irregular spherical shapes. The nanoparticles size are varied but the particles dimensions are between 30 to 90 nm. TEM analysis confirmed the SEM analysis, which illustrated the presence of nanoparticles in both spherical and irregular spherical geometries.

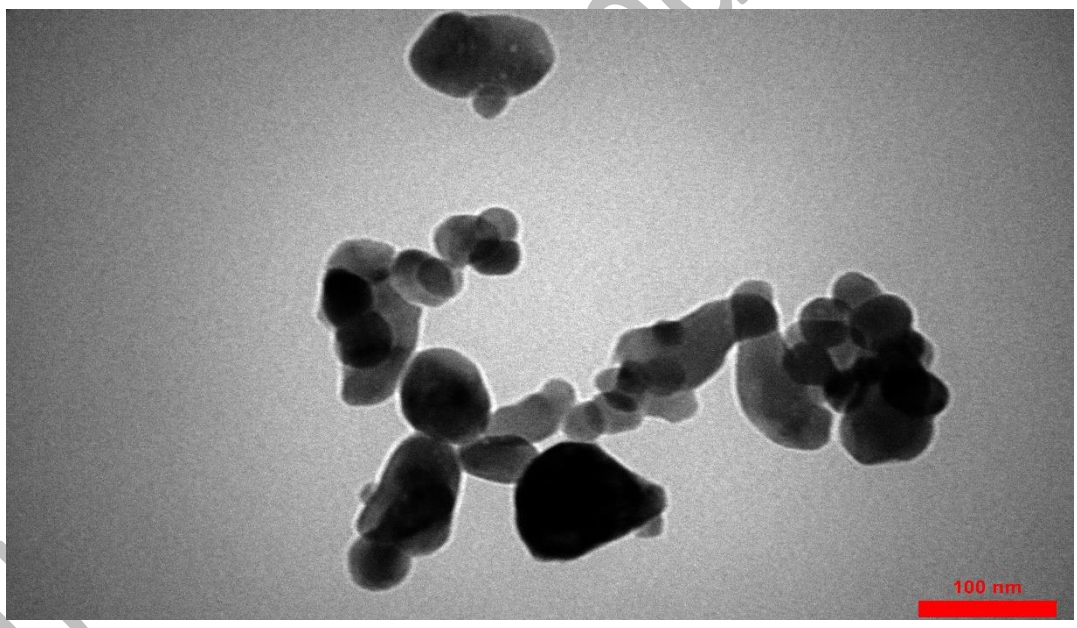

Figure 8. Error! Reference source not found.TEM image of prepared nanoparticles at 500°C (Ca-500)

3.7 Antibacterial activity of hydrophobic $CaCO_3$ nanoparticles

The antibacterial activity of $CaCO_3$ nanoparticles was studied by the disk diffusion method and the results are revealed in table 1. The antibacterial influence of $CaCO_3$ nanoparticles was clearly indicated by the existence of an inhibition zone. This zone revealed that the nanoparticles effectively inhibited the growth of bacteria, as observed through the disk diffusion method. As shown in table.1, antibacterial activity of hydrophobic $CaCO_3$ is higher than $CaCO_3$. Increasing the antibacterial activity of hydrophobic $CaCO_3$ compared to the hydrophilic $CaCO_3$ is due the interact of hydrophobic nanoparticles with the lipid bilayer of bacterial cell membranes that caused to disruption and subsequent cell death [36, 37]. According to the results, the mean inhibition zone

diameter in to hydrophobic and hydrophilic $CaCO_3$ case was increased by increasing the concentration of nanoparticles suspension. According to the results by increasing the concentration of $CaCO_3$ nanoparticles from 0.05 to 0.1 ml the inhibition zone increased. The results confirmed the growth of bacteria on the nanoparticle-free medium, and there was no evidence of bacterial inhibition. The experiments were repeated three times.

Sample	Bacteria	Nanoparticles dosage	Zone of Inhibition (mm) (Diameter)			
			1	2	3	Mean
$CaCO_3$ nanoparticles	Agrobacterium tumefaciens	0.05 ml	11	10	10	11.33
		0.1 ml	17	16	17	19
hydrophobic $CaCO_3$ nanoparticles		0.05 ml	15	15	16	11.33
		0.1 ml	25	25	26	19
nanoparticle-free medium		0 ml	0	0	0	0

Table 1. Antibacterial activity of $CaCO_3$ and surface modified $CaCO_3$

4. CONCLUSIONS

This study demonstrates that paper waste can be used as an inexpensive source to produce $CaCO_3$ antibacterial nanoparticles, serving as a means to reduce the accumulation of paper waste in landfills. Additionally, our conversion method is both simple and cost-effective. The XRD analysis indicated that the converting process of paper wastes to $CaCO_3$ nanoparticles was achieved in air environment in the lack of alkaline and acidic environment that in the alkaline environment the $CaCO_3$ structure and crystallinity decomposed. Furthermore, both XRD and SEM analysis revealed that increasing the calcination temperature caused to decreasing the crystallinity and increasing the crack on the surface of nanoparticles while the BET analysis confirmed this by indicating decreasing the surface area of Ca-750. This study illustrated the synergistic effect of stearic acid in surface modification of $CaCO_3$ nanoparticles and their antibacterial activity in decomposition of Gram-negative agrobacterium tumefaciens. This study showed the use of paper waste as a valuable source for the production of antibacterial $CaCO_3$ nanoparticles and revealed the successful surface modification of the produced nanoparticles for the creation of durable hydrophobic antibacterial coatings. These findings have significant implications for addressing corrosion issues in buildings and various industries. Further exploration and application of these nanoparticles in real-world settings could lead to the development of highly effective and long-lasting protective coatings.

Acknowledgements

The authors gratefully acknowledge Soran University and Nujan Nanofannavar Company for their complementary non-financial support.

REFERENCES

1. Liu, M., et al., *Waste Paper Recycling Decision System Based on Material Flow Analysis and Life Cycle Assessment: A Case Study of Waste Paper Recycling from China*. Journal of Environmental Management, 2020. **255**: p. 109859.
2. Zhang, Y. and S. Kudva, *E-Books Versus Print Books: Readers' Choices And Preferences Across Contexts*. Journal of the Association for Information Science and Technology, 2014. **65**(8): p. 1695-1706.
3. Budnyk, O., et al., *Printed And E-Book: Problems Of Choice Of Modern Students Of The University*. Revista Tempos e Espaços em Educação, 2021. **14**(33): p. 1.
4. Li, W., et al., *Biomethane Production Characteristics, Kinetic Analysis, And Energy Potential Of Different Paper Wastes In Anaerobic Digestion*. Renewable Energy, 2020. **157**: p. 1081-1088.
5. Alam, I. and C. Sharma, *Degradation Of Paper Products Due To Volatile Organic Compounds*. Scientific Reports, 2023. **13**(1): p. 6426.
6. Ciesielczuk, T. and C. Rosik-Dulewska, *Decomposition Dynamics Of Cooking-Oil-Soaked Waste Paper In Media With Low Inorganic Nitrogen Content*. Archives of Environmental Protection, 2023: p. 85-93-85-93.
7. Shokri, A.J.C., *Employing Electro-Peroxone Process For Degradation Of Acid Red 88 In Aqueous Environment By Central Composite Design: A New Kinetic Study And Energy Consumption*. 2022. **296**: p. 133817.
8. Shokri, A., B.J.P.S. Nasernejad, and E. Protection, *Treatment Of Spent Caustic Wastewater By Electro-Fenton Process: Kinetics and Cost Analysis*. 2023. **172**: p. 836-845.
9. Dutta, S., et al., *Catalytic Valorisation Of Various Paper Wastes Into Levulinic Acid, Hydroxymethylfurfural, And Furfural: Influence Of Feedstock Properties And Ferric Chloride*. Bioresource Technology, 2022. **357**: p. 127376.
10. Assis, e.i., b. Gidudu, and e.m. Chirwa, *Hydrothermal Carbonisation Of Paper Sludge: Effect Of Process Conditions On Hydrochar Fuel Characteristics And Energy Recycling Efficiency*. Journal of Cleaner Production, 2022. **373**: p. 133775.
11. Yu, R., et al., *Extraction And Characterization Of Nano-Cellulose From Local Waste Paper Egg Trays*. Journal of Natural Fibers, 2022. **19**(14): p. 8582-8592.
12. egamberdiev, e. and s. norboyev, *Extraction Of Cellulose Nanocrystals From Secondary Paper Waste And Their Use In Paper Production*. Technical science and innovation, 2022. **2022**(3): p. 215-222.
13. Durairaj, A., et al., *Conversion Of Laboratory Paper Waste Into Useful Activated Carbon: A Potential Supercapacitor Material And A Good Adsorbent For Organic Pollutant And Heavy Metals*. Cellulose, 2019. **26**: p. 3313-3324.
14. Ye, T.-N., et al., *Converting Waste Paper To Multifunctional Graphene-Decorated Carbon Paper: From Trash To Treasure*. Journal of Materials Chemistry A, 2015. **3**(26): p. 13926-13932.
15. Raisi, A., et al., *A Soft Tissue Fabricated Using A Freeze-Drying Technique With Carboxymethyl Chitosan And Nanoparticles For Promoting Effects On Wound Healing*. 2020. **7**(4): p. 262-274.
16. Foroutan, S., et al., *A Porous Sodium Alginate-Casio 3 Polymer Reinforced With Graphene Nanosheet: Fabrication And Optimality Analysis*. 2021. **22**: p. 540-549.
17. Fadia, P., et al., *Calcium Carbonate Nano-And Microparticles: Synthesis Methods And Biological Applications*. 2021. **11**: p. 1-30.
18. Chen, X., et al., *Wormwood-Infused Porous-$CaCO_3$ For Synthesizing Antibacterial Natural Rubber Latex*. 2024: p. 129322.
19. Demina, P.A., et al., *Freezing-Induced Loading Of TiO_2 Into Porous Vaterite Microparticles: Preparation Of $CaCO_3$/TiO_2 Composites As Templates To Assemble Uv-Responsive Microcapsules For Wastewater Treatment*. 2020. **5**(8): p. 4115-4124.
20. Al-Azzawi, M.H. and E.J.J.T.E.J.o.H.M. Al-Kalifawi, *Antibacterial and Antibiofilm Activity of Calcite ($CaCO_3$) Nanoparticles Synthesized from Chicken Eggshell*. 2023. **90**(2): p. 2275-2282.
21. Liu, X., et al., *Synergy Of Steam Reforming And K_2co_3 Modification On Wood Biomass Pyrolysis*. Cellulose, 2019. **26**: p. 6049-6060.
22. Shokri, A.J.S. and Interfaces, *Using Mn Based On Lightweight Expanded Clay Aggregate (Leca) As An Original Catalyst For The Removal Of NO_2 Pollutant In Aqueous Environment*. 2020. **21**: p. 100705.
23. Ugochukwu, U.C., *Characteristics Of Clay Minerals Relevant To Bioremediation Of Environmental Contaminated Systems*, In *Modified Clay And Zeolite Nanocomposite Materials*. 2019, Elsevier. p. 219-242.
24. Hu, S., et al., *Transport Of Hydrogen Isotopes Through Interlayer Spacing In Van Der Waals Crystals*. 2018. **13**(6): p. 468-472.
25. Marchini, C., et al., *Nanocrystalline And Amorphous Calcium Carbonate From Waste Seashells By Ball Milling Mechanochemistry Processes*. 2023.
26. Hussein, A.I., et al., *Synthesis And Characterization Of Spherical Calcium Carbonate Nanoparticles Derived From Cockle Shells*. 2020. **10**(20): p. 7170.

27. Liendo, F., et al., *Optimization Of $CaCO_3$ Synthesis Through The Carbonation Route In A Packed Bed Reactor*. 2021. **377**: p. 868-881.
28. Akhtar, K., S.J.J.o.D.S. Yousafzai, and Technology, *Morphology Control Synthesis Of Nano Rods And Nano Ovals $CaCO_3$ Particle Systems*. 2019.
29. Said, F.A., et al., *Antibiotic Loading And Development Of Antibacterial Capsules By Using Porous $CaCO_3$ Microparticles As Starting Material*. 2020. **579**: p. 119175.
30. Singh, K. and S. Sawant, *Identification Of $CaCO_3$ Polymorphs Of Shellfish By Ftir Spectroscopy And Evaluation Of Metals Adsorption By Powdered Exoskeleton Shell*. Indian Journal of Geo-Marine Sciences (IJMS), 2022. **51**(04): p. 304-309.
31. Cai, G.-B., et al., *1,3-Diamino-2-Hydroxypropane-N, N, N′, N′-Tetraacetic Acid Stabilized Amorphous Calcium Carbonate: Nucleation, Transformation And Crystal Growth*. CrystEngComm, 2010. **12**(1): p. 234-241.
32. Oreibi, I., M.A. Habeeb, and R.S.A.J.S. Hamza, *Tailoring The Structural And Optical Features Of PVA/SiO_2-CuO Polymeric Nanocomposite For Optical And Gamma Ray Shielding Applications*. 2023: p. 1-13.
33. Wang, Y., et al., *The Competitive Adsorption Mechanism Of CO_2, H_2O And O_2 On A Solid Amine Adsorbent*. Chemical Engineering Journal, 2021. **416**: p. 129007.
34. Kazemi Hakki, H., et al., *Preparation And Study Of Photocatalytic Hydrophobic Surface-Modified TiO_2 Coatings In Degradation Of E. Coli And Various Azo Dyes*. Iranian Journal of Chemistry and Chemical Engineering, 2023.
35. Shokri, A.J.E.C., *Using $NiFe_2O_4$ As A Nano Photocatalyst For Degradation Of Polyvinyl Alcohol In Synthetic Wastewater*. 2021. **5**: p. 100332.
36. Phuong, P.T., et al., *Effect Of Hydrophobic Groups On Antimicrobial And Hemolytic Activity: Developing A Predictive Tool For Ternary Antimicrobial Polymers.* Biomacromolecules, 2020. **21**(12): p. 5241-5255.
37. Krasowska, A. and K. Sigler, *How Microorganisms Use Hydrophobicity And What Does This Mean For Human Needs?* Frontiers In Cellular And Infection Microbiology, 2014. **4**: p. 112.